Journal of Materials Chemistry A

ROYAL SOCIETY OF CHEMISTRY

PAPER

View Article Online
View Journal | View Issue

Cite this: J. Mater. Chem. A, 2023, 11, 21300

Guest-induced breathing mediated selective alcohol recovery from water by MIL-88A(Fe)†

Nagore Barroso,[a] Subhajit Dutta,[a] Jacopo Andreo,[a] Garikoitz Beobide,[ab] Oscar Castillo,*[ab] Antonio Luque,[ab] Sonia Pérez-Yáñez[ab] and Stefan Wuttke*[ac]

The recovery of alcohols from low-concentration aqueous solutions is of great interest due to the wide use of alcohols in industrial processes. In this regard, adsorption-based separation is considered a green and cost-effective alternative towards high-energy demanding processes, which have been traditionally used in the separation of alcohol/water mixtures. Therefore, in this work, the recovery of different alcohols (methanol, ethanol, *n*-propyl alcohol, isopropyl alcohol, *n*-butyl alcohol, *sec*-butyl alcohol, isobutyl alcohol, and *tert*-butyl alcohol) from water has been studied based on the adsorptive separation properties of a very flexible metal–organic framework (MOF): MIL-88A(Fe). The adsorption capacity of the material has been studied for different alcohols by the magnetic sustentation technique taking advantage of the paramagnetic iron(III) metal centers in the structure. Interestingly, the competitive adsorption studies between different alcohols aqueous mixtures (methanol/*tert*-butyl alcohol, methanol/isopropyl alcohol and *n*-butyl alco-hol/*tert*-butyl alcohol) revealed the dominance of hydrophobicity of the alcohol over the size and shape factor, resulting in higher preference toward the alcohols with higher number of carbons. In addition, theoretical studies were carried out in order to have a deeper understanding of the adsorptive performance of MIL-88A(Fe), which demonstrated that framework flexibility and diffusion play a key role in alcohol adsorption. PVDF@MIL-88A(Fe) membranes with different MOF loadings were prepared to address the processability aspect of MOF powder. The synergetic contributions from PVDF and MIL-88A(Fe) resulted in a higher adsorption capacity of the composite material compared to the performance of each component, independently. Such systematic and strategic utilization of flexible MOFs can provide a promising platform for challenging alcohol separation from water and environmental remediation technologies.

Received 12th July 2023
Accepted 11th September 2023

DOI: 10.1039/d3ta04110g

rsc.li/materials-a

Introduction

Global climate change along with rising fuel prices and depletion of natural fuel supplies have culminated in a huge demand for green renewable energy production in order to meet the enormous energy demands worldwide.[1–3] In this regard, biofuels are considered one of the most promising viable and environmentally benign alternatives, which can also bring down the huge dependence on fossil energy sources.[4,5] Typically, biofuel products are obtained from dilute mixtures of alcohol in water, which are currently produced from agricultural feedstocks, fermentation of molasses and algae farms. This inevitably requires the recovery of those alcohols from such diluted mixtures, which usually relies on the high energy demanding distillation and purification processes that also present a poor net energy balance (NEB), *i.e.* the difference between the energy generated from the fuel and the production energy consumption is only ~25%.[6–8] Moreover, ethanol and water form an azeotropic mixture from which ~4% of the water is impossible to remove using the conventional distillation process.[4] Hence recovery of alcohols from low-concentration aqueous solutions is still challenging and highly important from an energy-economic point of view.[9] Short-chain alcohols present many valuable applications and technological relevance. Apart from the ubiquitous ethanol, methanol is also a major alcoholic component having a huge importance in various industrial sectors. For instance, methanol is an industrial feedstock in the production of insecticides. It is also employed as feedstock to manufacture several other industrial products such as methanal (formaldehyde), acetic acid, methyl esters of various acids and so on. However, because of its intrinsic toxic nature, methanol and its distillation wastes are classified as HW42 hazardous waste and possess high threat to the atmosphere, soil and groundwater.[10] Long-term ingestion of

[a]BCMaterials, Basque Center for Materials, Applications and Nanostructures, UPV/EHU Science Park, 48950 Leioa, Spain. E-mail: oscar.castillo@ehu.eus; stefan.wuttke@bcmaterials.net

[b]Organic and Inorganic Chemistry Department, University of the Basque Country, UPV/EHU, Barrio Sarriena s/n, 48950 Leioa, Spain

[c]IKERBASQUE, Basque Foundation for Science, 48009 Bilbao, Spain

† Electronic supplementary information (ESI) available. See DOI: https://doi.org/10.1039/d3ta04110g

methanol contamination can lead to some diseases like blindness, chronic nerve damage and even death. Therefore, the development of novel porous materials for efficient methanol removal from water, even at low concentrations, is a pressing environmental need.

In this regard, adsorptive separation-based techniques have established themselves as green and cost-effective alternatives to the high-energy footprint of the traditional distillation processes.[11,12] To date, several porous sorbent materials such as zeolites, organic polymers or activated carbons have been employed for such separation applications. However, several limitations like poor selectivity, lower sorption efficiency and high regeneration cost necessitate development of next-generation porous sorbents with enhanced efficiency.[13,14] In this context, metal–organic frameworks (MOFs) have attracted significant scientific attention as they offer superior sorption performance as well as enhanced selectivity toward targeted sorbate species.[15] MOFs are a class of three-dimensional crystalline frameworks built up from the assembly of inorganic building units (IBUS) and organic building units (OBUs) that are linked through strong coordination bonds.[16,17] They exhibit high surface areas, large porosity and tunable structures due to the wide range of available chemical inorganic–organic combinations.[18–22] Overall, these outstanding properties make MOFs very suitable materials, especially for volume specific applications such as purification, separation or adsorption processes.[23–26] Over the last decades MOF field have increased sharply, leading to a deep understanding of the field, which together with the discovery of many different structures such as breathing MOFs, have attracted great interest.[27–32] Unlike rigid frameworks, flexible MOFs exhibit structural dynamism arising from physical (temperature, pressure, light) or chemical (guest incorporation or elimination) external stimuli.[31,33–40] Among the flexible MOFs, MIL-88A outstands due to the large breathing transformation, cost effectiveness or easy synthesis. MIL-88A presents a hexagonal-type structure built up from oxo-centred iron(III) octahedral trimers connected by dicarboxylates groups from the fumarate anion, forming an interconnected 3D structure.[41,42] The O–O axis of the carboxylate groups allows the rotation of both metal clusters and organic linker,[34] making MIL-88A one of the largest breathing MOF ever reported.[29] In this sense, the adsorption/desorption of guest molecules in the MOF is accompanied with an expansion/contraction of the unit cell, while the space group is maintained.[43] Such flexibility of MIL-88A series proven to be beneficial for various applications. For example, effect of flexible character of MIL-88 Fe(III) was exploited for selective adsorption of *n*-alkanes.[44] The guest-induced breathing of MIL-88 also have been employed toward adsorption of biologically active nitric oxide (NO) species.[45] The breathing effect was also exploited for remediation of various toxic water pollutants such as heavy metals,[46] pharmaceuticals and personal care products (PPCPs)[47] and dyes.[48] Despite these efforts, the potential of guest-induced framework adaptability of MIL-88A(Fe) toward liquid separation challenges such as the recovery of alcohols from aqueous environments is still untapped.

In order to close this scientific gap, herein, the recovery of short-chain aliphatic alcohols from water has been studied with MIL-88A(Fe) MOF in order to address the challenge of alcohol-water separation (Fig. 1). Specifically, 1 to 4 carbon-containing aliphatic alcohols has been used: methanol, ethanol, propyl alcohol (*n*- and iso-isomers) and butyl alcohol (*n*-, *sec*, iso-, and *tert*-isomers), herein denoted as MeOH, EtOH, *n*-prOH, i-prOH, *n*-buOH, *sec*-buOH, i-buOH, and i-buOH, respectively. The single-component alcohol adsorption experiments showed a linear tendency for the adsorption of linear alcohols, where the adsorption capacity of MIL-88A(Fe) was found to be higher for smaller molecules (methanol), while branched alcohols showed more modest values. Theoretical studies corroborate well with the fact that such differential adsorption behavior is attributed to the flexible nature of the MOF structure allowing the diffusivity of small molecules, while hindering the diffusion of branched alcohols. Interestingly, the competitive adsorption studies contrast with the single-component alcohol adsorption experiments, where a clear preference towards more hydrophobic molecules (isopropyl alcohol or *tert*-butyl alcohol) was observed over methanol. Difference in polarity of the incoming alcohol molecules found to dictating the sorption process in case of the multicomponent sorption studies. Finally, PVDF@MI-88A(Fe) mixed matrix membranes were prepared to address the real-time applicability aspect of the MOF powders. The combination of guest-selective adaptable breathing effect along with selective host–guest interaction proven to be highly potent for MIL-88A toward selective and efficient recovery of alcohols from water even in the low concentration liquid mixtures.

Experimental procedure

Synthesis of the materials

MIL-88A(Fe). MIL-88A(Fe) was synthesized according to an already reported protocol.[41,48] Briefly, iron(III) chloride hexahydrate (1.381 g, 5.11 mmol) and fumaric acid (0.593 g, 5.11 mmol) were dissolved in a mixture of 25 mL of solvent DMF : water (1 : 1, v/v). The reaction mixture was placed in a preheated oven at 65 °C for 4 hours. The compound was recovered by centrifugation and washed (15 000 rpm, 15 min, 36 mL) two times in water. Further washing steps were carried out soaking the particles for 1 h in ethanol over 3 days.

PVDF@MIL-88A(Fe) membrane preparation. PVDF@MIL-88A(Fe) membranes with different MOF loadings (0, 10, 20 and 30 wt%) were prepared following doctor blade and NIPS procedure according to already reported protocols.[49,50] Briefly, to an initial suspension of MIL-88A(Fe) microparticles in DMF (6 mL), PVDF powder was gently added to prevent agglomeration while stirring (2 h) and ensuring its complete dissolution. The amount of MOF and polymer employed were adapted to obtain a total mass of 1 g. Then, the colloids were spread onto a glass substrate using a doctor blade with a fixed thickness of 250 μm in order to obtain thin films of the composite. The membrane was detached from the glass substrate by immersing it in a water bath at 75 °C and afterwards, it was left 30 min in MIL-88A(Fe) viewed along *c* axis. Pore size distribution of the (c)

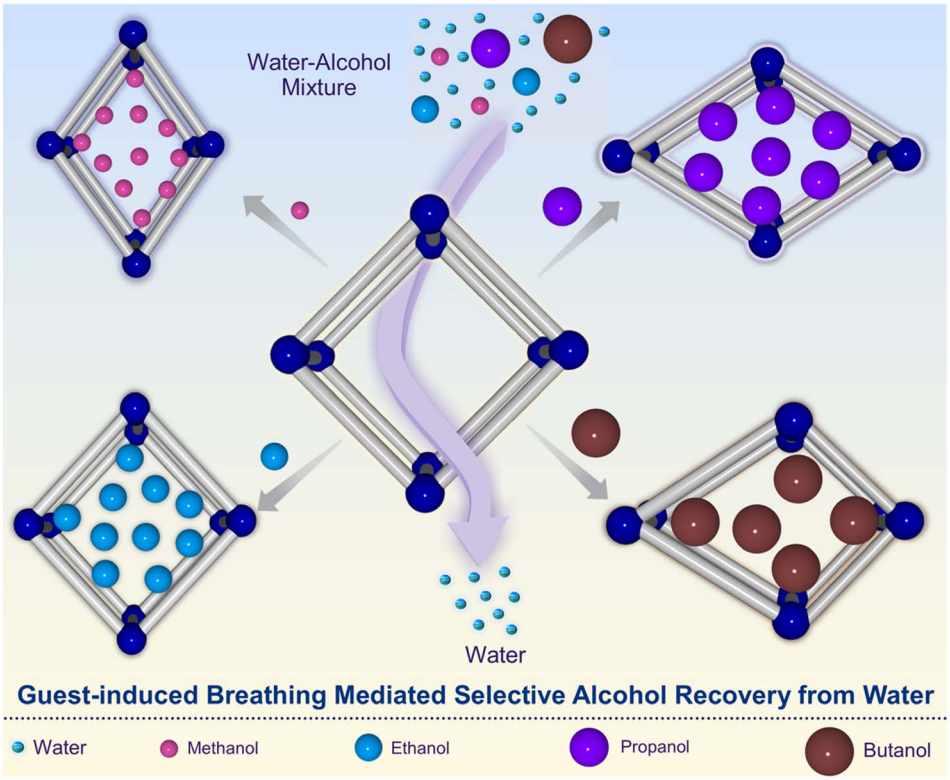

Fig. 1 Schematic illustration of the guest-induced MOF breathing mediated alcohol recovery from aqueous solution.

open another water bath at room temperature to remove all the DMF. Finally, membranes were allowed to dry overnight at room temperature.

Results and discussion

Alcohols sorption from aqueous media

As mentioned in the introduction, the crystal structure of MIL-88A(Fe) can switch between open and closed forms (Fig. 2a–d). The PXRD pattern of the as-synthetized micron-size rod-like shape samples revealed an intermediate state between the open and close forms (Fig. 2e). This intermediate state was previously observed by Troyano *et al.*[51] when MIL-88A(Fe) was exposed to different humidity atmospheric conditions. In this study, the sorption experiments were performed in aqueous media and thus, the as-synthesized MIL-88A(Fe) sample transits to the open form configuration (Fig. 2e). Therefore, the results obtained in all the adsorption experiments must be understood regarding pore dimensionality and connectivity of the open form.

The quantification of the captured alcohols from aqueous media was performed using a recently developed technique named magnetic sustentation (Fig. S1†).[52,53] It is based on the paramagnetic nature of the metal centers of MOFs and their interaction with a variable magnetic field. The captured amount of the targeted molecules from solution can be characterized based on the change in the critical magnetic field at which the paramagnetic MOF particles are detached from the pole of the

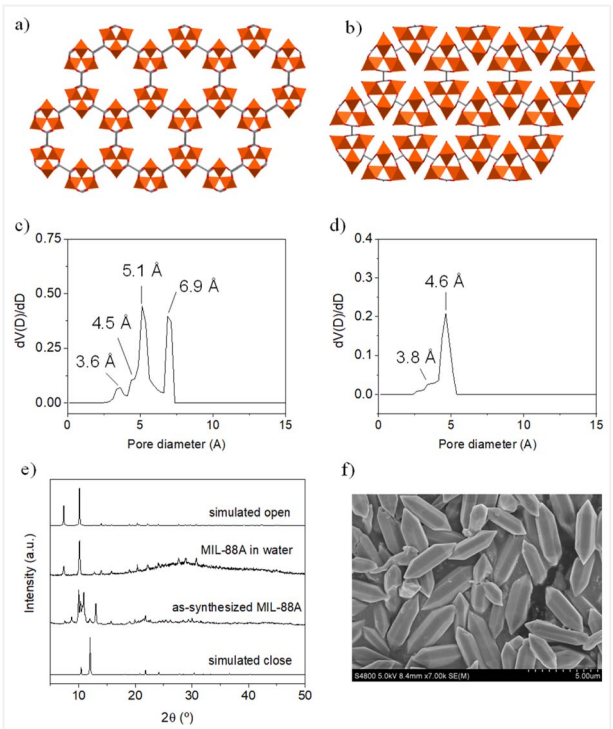

Fig. 2 Schematic representation of the (a) open and (b) close forms of MIL-88A(Fe) viewed along *c* axis. Pore size distribution of the (c) open and (d) close forms computed using Poreblaze 4.0. (e) PXRD patterns of the as synthesized and in water soaked sample and simulated open and close forms. (f) FESEM images of as-synthesized MIL-88A(Fe).

electromagnet. This change is linearly correlated with the adsorbed mass percentage of the captured molecule. The technique offers several advantages towards more conventional techniques (UV-vis spectroscopy or ^{1}H-NMR) such as the direct quantification of the adsorbate mass incorporated into the MOF. In addition to that, the technique does not present any dependence on the nature of the adsorbate. The theoretical equations describing the magnetic sustentation phenomenon, indicate that there is a linear dependence between the critical magnetic field, H, and the adsorbed mass, according to eqn (1):

$$M_{M(F)} = A' \cdot H - B' \quad (1)$$

where, $M_{M(F)}$ corresponds to the captured mass of the adsorbate in the framework, H is the critical magnetic field determined from magnetic sustentation experiments and A' and B' are constant values.

The critical magnetic field of the pristine paramagnetic MIL-88A(Fe) (named MIL-88A(Ø)) and after the adsorption of the short chain alcohols (methanol, ethanol, *n*- and isopropyl alcohol, *n*-, *sec*-, iso- and *tert*-butyl alcohol) in water was determined (Fig. 3a). Briefly, MIL-88A(Fe) particles were dropped in a test tube located between the two poles of an electromagnet and subjected to its maximum magnetic field. The paramagnetic particles were attached to the walls of the test tube in the lower part of the electromagnet pole, where the magnetic force is maximum. Afterwards, the generated magnetic field is progressively reduced until the particles are detached. The magnetic field value at this point is denoted as the critical magnetic field of eqn (1).

The alcohol capture from water was performed by placing MIL-88A(Fe) in an aqueous solution containing 50 μL of each alcohol. The resulting suspension was kept under agitation for 24 h. Later, MIL-88A(Fe) microcrystals were recovered by centrifugation and the captured amount of alcohol was quantified. The critical magnetic field of MIL-88A(Fe) before alcohol adsorption was labelled as Ø. As observed in Fig. 3a, the critical magnetic field of MIL-88A(Fe) after adsorption of short chain alcohols increased compared to the pristine MOF(Ø); the bigger the deviation from the pristine material the higher the mass percentage incorporated in the MOF suggesting that MIL-88A(Fe) can efficiently capture alcohols from water. A calibration curve was established using MIL-88A(Fe)(Ø), DMSO and DMF adsorbed samples, whose adsorption values were determined independently by UV-vis spectroscopy (see Fig. S2† for additional details). The extrapolated adsorption values are detailed in Fig. 3b. As expected, the smaller the adsorbate molecules the greater the adsorption showing the highest value for methanol (3.56 molecules per MOF formula) and the lowest for *tert*-butyl alcohol (0.31 molecules per MOF formula). Such vast difference (~10 times) in adsorption capacity between different alcohols (MeOH and t-BuOH) is indicative of differential intermolecular interactions and structural preference of MIL-88A(Fe) toward incoming guest molecules. Interestingly, MIL-88A(Fe) exhibited greater sorption toward *n*-BuOH (0.9 molecules per MOF formula) in comparison with other BuOH variants, *i.e.* i-BuOH (0.4 molecules per MOF formula) and *t*-BuOH (0.31 molecules per MOF formula). ^{1}H-NMR was also employed to validate the sorption behavior toward the highest and lowest adsorbed molecules, *i.e.* methanol and *tert*-butyl alcohol, respectively (Fig. S3–S5†). In addition, the adsorption experiments were repeated and quantified using 200 μL of the alcohols. The results indicated no significant differences in the adsorption values, suggesting that MIL-88A(Fe) was already saturated at 50 μL (Table S1†). Furthermore, a study of the adsorption kinetic was also completed for MeOH to ensure that the established 24 h for the adsorption procedure is enough for the system to achieve the equilibrium state (Fig. 3c), in order to address the possible concerns about the process being governed by thermodynamic or kinetic factors.[54,55] The methanol adsorption after 24 h was measured both using water and the same diluted MeOH aqueous solution to ensure the critical magnetic field measurement is not affected by the change in the liquid media employed. As shown in the inset of Fig. 3c, no significant change was observed.

This means that the obtained values should reflect the complementarity between the shapes of the adsorbate molecules and the voids in the open form of MIL-88A(Fe). In this sense, we have performed a computational characterization,

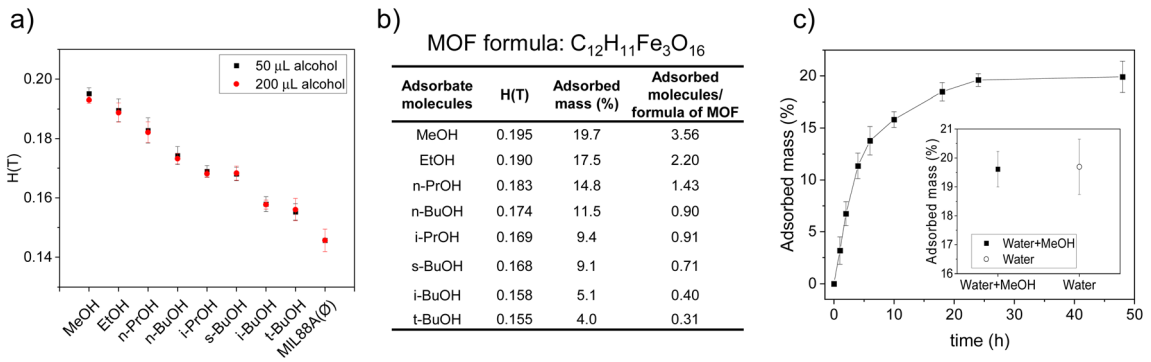

Adsorbate molecules	H(T)	Adsorbed mass (%)	Adsorbed molecules/ formula of MOF
MeOH	0.195	19.7	3.56
EtOH	0.190	17.5	2.20
n-PrOH	0.183	14.8	1.43
n-BuOH	0.174	11.5	0.90
i-PrOH	0.169	9.4	0.91
s-BuOH	0.168	9.1	0.71
i-BuOH	0.158	5.1	0.40
t-BuOH	0.155	4.0	0.31

Fig. 3 (a) Critical magnetic field of MIL-88A(Fe) after adsorption of alcohols determined by magnetic sustentation experiments. (b) Quantification of the adsorbed alcohols: critical magnetic field, $H(T)$, adsorbed mass (%) and adsorbed molecules per formula of MOF. (c) Kinetic of the adsorption for methanol (inset figure: determination of the critical magnetic field after 24 h, using water or methanol aqueous solution as measurement media).

using the Materials Studio suite platform. The configuration for each alcohol was optimized to provide the less sterically hindered conformation (Fig. 4a). The molecular volume and cross section of the alcohols on these optimized conformations were calculated using a 1.2 Å molecular probe. The same molecular probe was employed to characterize the big cavity and connecting windows dimensions. The pore system within the open form of MIL-88A(Fe) is composed of two big cavities around 6.9 and 5.1 Å connected by slightly narrower windows (diameter: 4.4 and 3.6 Å) to generate an interconnected 3D channel system. In a rigid crystal structure, the diffusion-limiting factor should be the cross sections of these windows. Nonetheless, the flexible nature of the crystal structure of MIL-88A(Fe) allows the diffusion of alcohol molecules with slightly greater cross-sections, as happened for linear alcohols. However, this structural flexibility is limited and above certain cross-section values, the diffusion of the alcohol molecules is hindered resulting in significantly lower adsorption values. The latter is the case of the branched alcohols. In Fig. 4b and c the adsorption values are plotted against the calculated molecular volume and cross section, respectively. A linear tendency can be observed between the captured mass and molecular volume of linear alcohols (methanol, ethanol, *n*-propanol and *n*-butyl alcohol), which can be attributed to a more efficient occupation of the voids by smaller molecules. In contrast, the adsorbed mass of branched alcohols (isopropyl alcohol, *sec*-butyl alcohol, isobutyl alcohol and *tert*-butyl alcohol) shows a linear dependence with respect to the cross section, which in this case it seems to be the limiting factor as the diffusion of the molecules seems to play a crucial role. Although the molecular volumes of isopropyl alcohol and sec-butyl alcohol are significantly different, they have similar cross sections, which results in similar adsorption values. In addition, the similar cross-section for iso- and *tert*-butyl alcohols give rise to similar adsorption values. Overall, it can be concluded that the molecular volume of the alcohols is the key factor determining the adsorption of linear alcohols (relatively small cross-section), while for branched alcohols, where bigger cross-sections are shown, this latter parameter becomes the dominant one.

In order to provide more evidence to support this explanation, further computational studies were carried out. The pore structure was analyzed by GCMC calculations (Fig. S6† shows the MOF fragment used for the DFT calculations, while Table S2† gathers the resulting charges) using methanol and *tert*-butyl alcohol as molecular probes. Fig. 5 showed the probability density maps probed by a single-molecule (*i.e.* fixed loading calculations) in a 2 × 2 × 2 supercell of the open form of MIL-88A(Fe) computed at 298 K.

Methanol molecule shows percolation along the entire three-dimensional pore network. Despite *tert*-butyl alcohol can also fit into the bigger cavities of the open form structure, it shows occupational discontinuities in the vicinity of the windows that create the above explained diffusional problem of the branched alcohols. On the other hand, the calculations performed at fixed pressure (100 kPa at 298 K) led to loadings of 130 methanol molecules and 49 *tert*-butyl alcohol molecules per supercell,

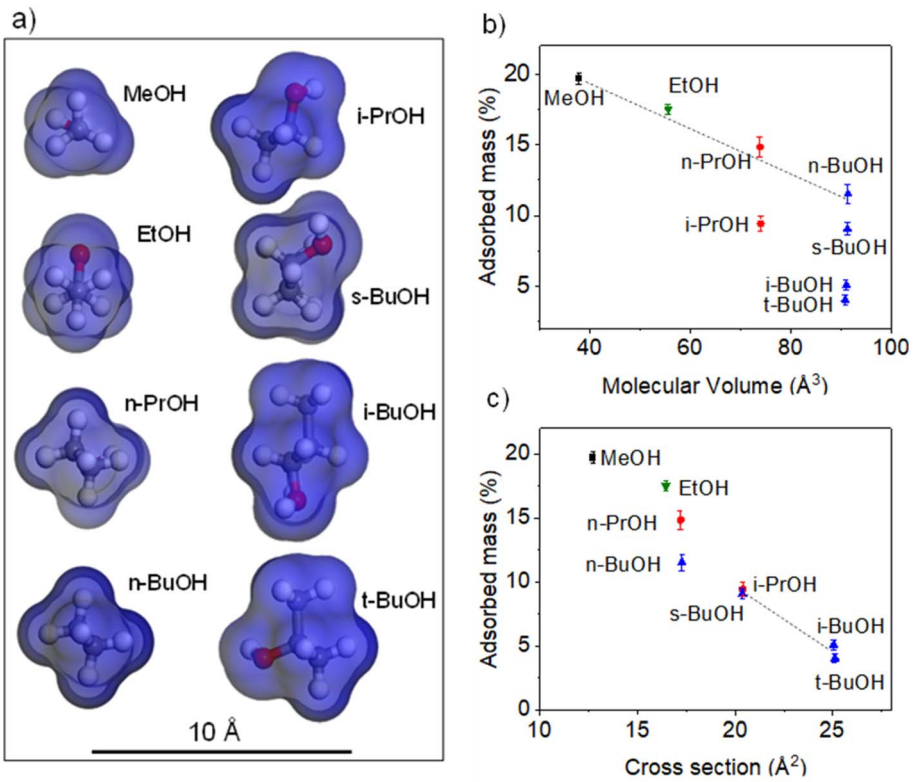

Fig. 4 (a) Optimised configuration of the alcohols drawn with "Materials Studio Suite". Adsorbed mass (%) for each alcohol plotted against (b) molecular volumes and (c) cross sections.

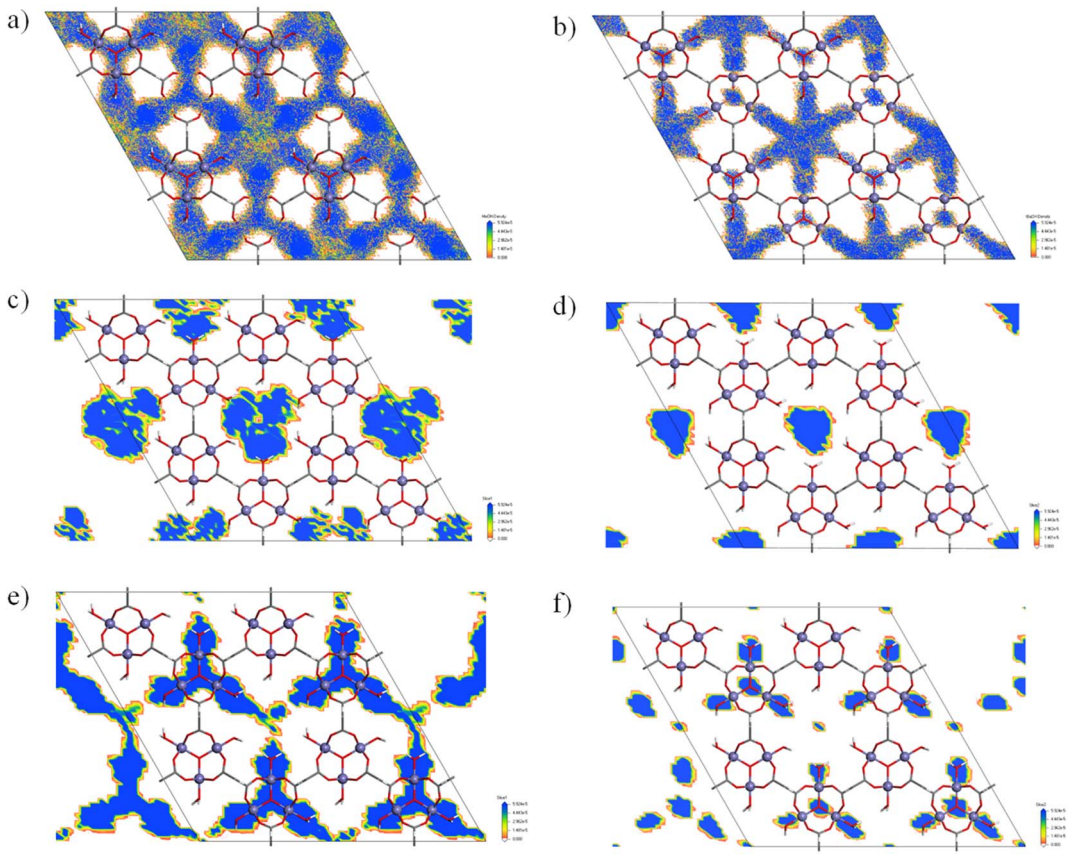

Fig. 5 Fixed loading calculations (1 molecule per cell at 298 K) for methanol (left) and *tert*-butyl alcohol (right): probability density distribution and its projection: (a and b) for plane (001), (c and d) at $z = 0.5$ and (e and f) $z = 0.375$.

which correspond to approximately 8 methanol molecules and 3 *tert*-butyl alcohol molecules per formula. These values are higher than the experimental ones (3.5 and 0.3 molecules of methanol and *tert*-butyl alcohol, respectively). In the case of methanol, this discrepancy can be attributed to the fact that the experimental adsorption experiment involves a competition between water and alcohol molecules to occupy the pores of the compound. In the experimental, this competition reaches the equilibrium, in which probably a mixture of water and alcohol molecules occupies the pores. However, the computational studies consider the occupation of the voids of the only alcohol molecules. As consequence, a higher adsorption capacity is computed compared to results obtained from the single alcohol adsorption experiments in water. This fact was corroborated with the vapour phase alcohol sorption performance of MIL-88(Fe) in which approximately 12.6 methanol molecules and 2.3 *tert*-butyl alcohol molecules per formula are adsorbed (Fig. 6a). These values are higher than those obtained in aqueous solution (3.56 and 0.31 molecules per formula of MOF for methanol and *tert*-butyl alcohol, respectively) owing to the existing competition between alcohol and solvent (water) molecules, resulting in sorption performance. However, such competitive adsorption can play important role in the reduction of adsorption capacity observed with both, methanol and *tert*-butyl alcohols, the difference is not that evident for *tert*-butyl

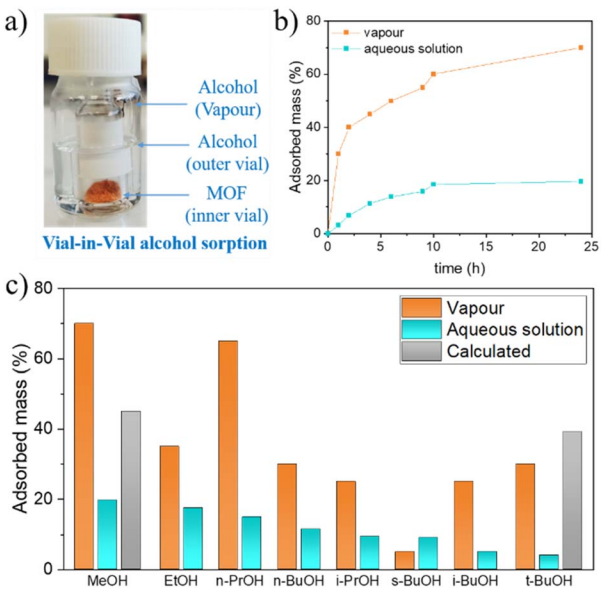

Fig. 6 (a) Pictorial representation of "vial-in-vial" vapour phase alcohol sorption experiments setup. (b) Adsorption kinetics curves for MeOH in vapour and aqueous solution. (c) Comparative alcohol adsorption values when performing the experiments in aqueous solution, from gas-phase or by GCMC theoretical calculations.

alcohol (0.3 molecules per formula of MOF in solution *vs.* 3.1 and 5.4 obtained from theoretical calculations and vapour adsorption, respectively), which could be attributed to diffusion problems limiting the adsorption of branched alcohols. In fact, the correlation between the adsorption in solution and the cross-section of the branched alcohols described above seems to agree with this. Furthermore, the MeOH adsorption kinetic curves prepared for both, aqueous solution and vapour (Fig. 6b), indicate a faster diffusion of the alcohol molecules into the pores of MIL-88(Fe) in vapour (300 mg of MeOH g^{-1} h^{-1}), than in solution (32 mg of MeOH g^{-1} h^{-1}), even though the adsorption implies a structural rearrangement. This fact is indicative of the presence of water molecules in the pores prior to the entrance of alcohol molecules hindering their diffusion. Therefore, the reduced adsorption of *tert*-butyl alcohol obtained from the experimental results must be understood as a probe of the presence of a diffusion problem and not due to an absence of big enough pores that could fit *tert*-butyl alcohol. Finally, Fig. S7† shows a low energy distribution of guest alcohol molecules at MIL-88A(Fe), where both alcohols show similar adsorption preferential sites. On the whole, it can be concluded that even if similar preferential adsorption sites are observed for both molecules, the flexibility of the structure is what limits the diffusion and thus, the loading of *tert*-butyl alcohol. However, to better understand the main reason behind the noticeable decrease of the "in solution" adsorption capacity in case of the branched alcohols, we have executed additional competitive adsorption experiments that will be discussed later. The MIL-88A(Fe) samples resulting from the adsorption experiments were further characterized by PXRD while they were still wet, which to the best of our knowledge it was not previously studied. The wet samples were subjected to a series of consecutive scans with an interval of 10 min in order to observe the evolution of their PXRD patterns upon the release of the adsorbed alcohol molecules (Fig. S8†). In all cases, the initial diffractograms show the amorphous contribution of water wetting the solid particles, together with the typical diffraction peaks of the open form of MIL-88A(Fe). Over time, the amorphous contribution decreases in agreement with the expected evaporation of the solvent (water). Finally, after the drying of the sample (water evaporation) and the release of the captured alcohols molecules, the diffractogram evolve to the initial intermediate structure of MIL-88A(Fe). The recyclability and stability of MIL-88A(Fe) were studied measuring the adsorption capacity of the material up to four cycles, in which the alcohol molecules were desorbed in between the cycles under high vacuum. Overall, it can be concluded that there is no significant change in its adsorption capacity (Fig. S9c†). PXRD and ATR FT-IR measurements were performed after the first and last cycle to ensure the structural and chemical stability of MIL-88A(Fe) (Fig. S9†), showing no significant change.

Competitive adsorption studies

Simultaneous and consecutive competitive adsorption studies were performed to further study the behavior of MIL-88A(Fe) (Fig. 7a). Simultaneous competitive adsorption studies were performed to study the affinity of MIL-88A(Fe) towards different alcohols. Three different mixtures were prepared containing an equimolar amount of each alcohol: (A) combination of the two most diverse alcohols (methanol/*tert*-butyl alcohol), (B) combination of the two widely employed alcohols (methanol/isopropyl alcohol) and (C) combination of the linear and branched alcohols with the same number of carbons (*n*-butyl alcohol/*tert*-butyl alcohol). ^{1}H-NMR was used to quantify the remaining amount of alcohol in solution after 24 h of adsorption (Fig. S10–S12†). The amount of alcohol in solution was reduced from the employed in the magnetic sustentation experiments in order to ensure that the variation of the alcohol in the remaining liquid could be reliably quantified by ^{1}H-NMR. This fact also explains the relatively lower adsorption values obtained in these latter experiments. The obtained values from the simultaneous competitive adsorption experiments are depicted in Fig. 7b and c. The results of the competitive studies

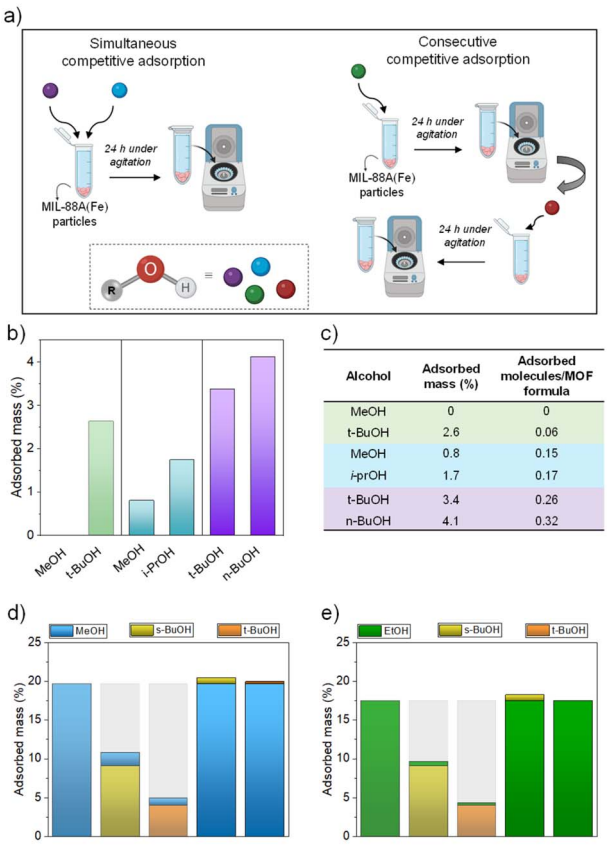

Fig. 7 (a) Schematic representation of the simultaneous and consecutive competitive adsorption. Competitive adsorption studies for MIL-88A(Fe): (b) adsorbed mass (%) of alcohols and (c) values of the adsorbed mass (%) and adsorbed molecules per formula of MOF in equimolar mixtures (A) (methanol/*tert*-butyl alcohol), (B) (methanol/isopropyl alcohol) and (C) (*tert*-butyl alcohol/*n*-butyl alcohol)). Consecutive adsorption studies for MIL-88A(Fe): (d) methanol, branched alcohols + methanol and methanol + branched alcohols and (e) ethanol, branched alcohols + ethanol and ethanol + branched alcohols. Note that the alcohol at the bottom of each bar corresponds to the first adsorption step followed by the adsorption of the second alcohols in the consecutive single alcohol adsorption experiments.

indicate that the adsorption preference is directed by the hydrophobicity of the alcohol and not by size or shape factor as observed from the single alcohol adsorption experiments. Although methanol showed the highest adsorption in the single adsorbate experiments, there is a clear preference for more hydrophobic molecules, *tert*-butyl alcohol and isopropyl alcohol. In addition to that, the amount of captured *tert*- butyl alcohol is very modest, in agreement with the results from the single alcohol experiments, which implies that there is still a lot of free space in the pore system of the open form of MIL-88A(Fe) that apparently are not further accessible after the incorporation of *tert*-butyl alcohol molecules. The explanation for this phenomenon relies again on the diffusional problems of *tert*-butyl alcohol (and to a lower extent, isopropyl alcohol) within the pore system of MIL-88A(Fe). The diffusion problems do not only affect the adsorption values of *tert*-butyl alcohol, which are quite modest, but also the adsorption of any other molecules that have to deal with increasing diffusion difficulties arising from those branched alcohol molecules clogging the pore system. Moreover, it also implies that the more hydrophobic molecules are the first ones coming out from the aqueous solution to start interacting with the MIL-88A(Fe) particles. Finally, *n*-butyl alcohol and *tert*-butyl alcohol isomers, with similar affinity towards MIL-88A(Fe), have similar adsorption values as both alcohols compete in relatively equal terms.

In order to get further insight into this clogging phenomenon that the branched alcohols seem to create, a series of additional adsorption experiments were designed in which two 24 h consecutive single alcohol adsorption experiments were performed alternating between branched (*t*-BuOH and *s*-BuOH) and small linear alcohols (MeOH and EtOH). The results showed a striking difference depending on the order of the addition of alcohols (Fig. 7d and e). The high adsorption values observed in the single alcohol adsorption experiments for MeOH and EtOH showed a slight increase when the branched alcohols are added in the second step. However, the very modest adsorption values of the branched alcohols are retained even after the exposure to the short chain alcohols in the second step. This behavior can also be attributed to the clogging of the pore system of MIL-88(Fe) caused by the branched alcohols, which hinders the adsorption of MeOH or EtOH leading to a far smaller amount incorporated in the framework. Another feature that seems to agree with the hypothesis of pores clogging is that the small increase observed after the second addition follows the expected order. The overall increase after the second step is higher when, in the first step, the less hindering *s*-BuOH is employed over *t*-BuOH. On the other hand, the increase after the second addition is in both cases higher for the smaller MeOH than for the bigger EtOH.

Moreover, the hypothesis of the clogging effect was validated determining the kinetic desorption curves of linear (MeOH) and branched alcohols (*t*-BuOH), together with the consecutively adsorbed alcohols, where the linear alcohol was adsorbed first (MeOH + *t*-BuOH). To confirm the diffusional problem generated by *t*-BuOH, a significant decrease on the desorption rate of MeOH + *t*-BuOH should be observed compared to the desorption rate of MeOH. In other words, the clogging effect should hinder both the incorporation (as proved before) and the release. Fig. S10† shows the desorption curves, in which the above predicted behaviour is clearly observed. In addition to that, the desorption rate of MeOH + *t*-BuOH samples during the first 4 hours of the experiments shows a similar behaviour to *t*-BuOH, indicating that the adsorption of the branched alcohol is the determining factor dictating the slower release due to the clogging of the pores.

PVDF@MIL-88A(Fe) composite membranes

Although MOFs show good adsorptive performances due to their high surface areas and porosity, they are obtained as fine powders, which limits their practical applications.[56,57] Among the main disadvantages of using MOFs as powder the limited packing densities, high diffusion barriers and difficulties to recover the material from solution can be found. In order to overcome these problems, the use of MOFs as fillers in polymeric mixed matrix membranes have been proposed.[58–60] Over the last years, polymer@MOF membranes have been widely reported for the removal of metal ions in water[61,62] dye wastewater[63,64] or oil pollution.[65,66] Although there are many different polymeric materials available, polyvinylidene fluoride (PVDF) has been widely used due to the high chemical and thermal stability, easy processing, high organic selectivity or hydrophobicity.[67,68] Therefore, to overcome one of the limiting factors of MOF powders in practical applications, *i.e.* the processability, the use of MIL-88A(Fe) as filler in a polymeric matrix was explored. PVDF@MIL-88A(Fe) composite membranes with different MOF loadings (0, 10, 20, 30 wt%) were prepared (Fig. 8) according to the procedure described in the experimental section.

SEM images (surface and cross-section) of the membranes confirm that MIL-88A(Fe) microcrystals were homogeneously dispersed within the porous PVDF matrix without any sign of agglomeration (Fig. 8a–l). The dimensions of the macropores within the polymeric matrix changed with the loaded amount of MIL-88A(Fe) showing an average pore size of 0.49 ± 0.11 μm, 0.96 ± 0.39 μm, 1.51 ± 0.47 μm, and 0.51 ± 0.26 μm, for the 0, 10, 20 and 30 wt% MOF-loaded membranes, respectively. Higher content of MOF in the PVDF membranes up to a 20 wt% increased the size of the pores, except for the 30 wt% MOF-loaded membrane, whose pores are comparable to those of the 0 wt% membrane. In addition, PXRD patterns of the membranes also confirm the successful incorporation of MIL-88A(Fe) into the matrix as no significant changes were appreciated between the different MOF loadings (Fig. 8m). The membranes were further characterized by thermogravimetric and contact angle analyses (Fig. S14†). TGA measurements of the membranes show the expected mass loss around 215 °C corresponding to MIL-88A(Fe) and a more pronounced mass loss around 315 °C corresponding to PVDF. The latter appears at a lower temperature compared to the pure PVDF (370 °C), which can be attributed to the increased porosity of the MOF-incorporated membranes. This trend has also been previously reported for other PVDF composites.[49,69,70] The mass percentage of the residue at 800 °C, corresponding to Fe_2O_3 (PDF 89-0597),

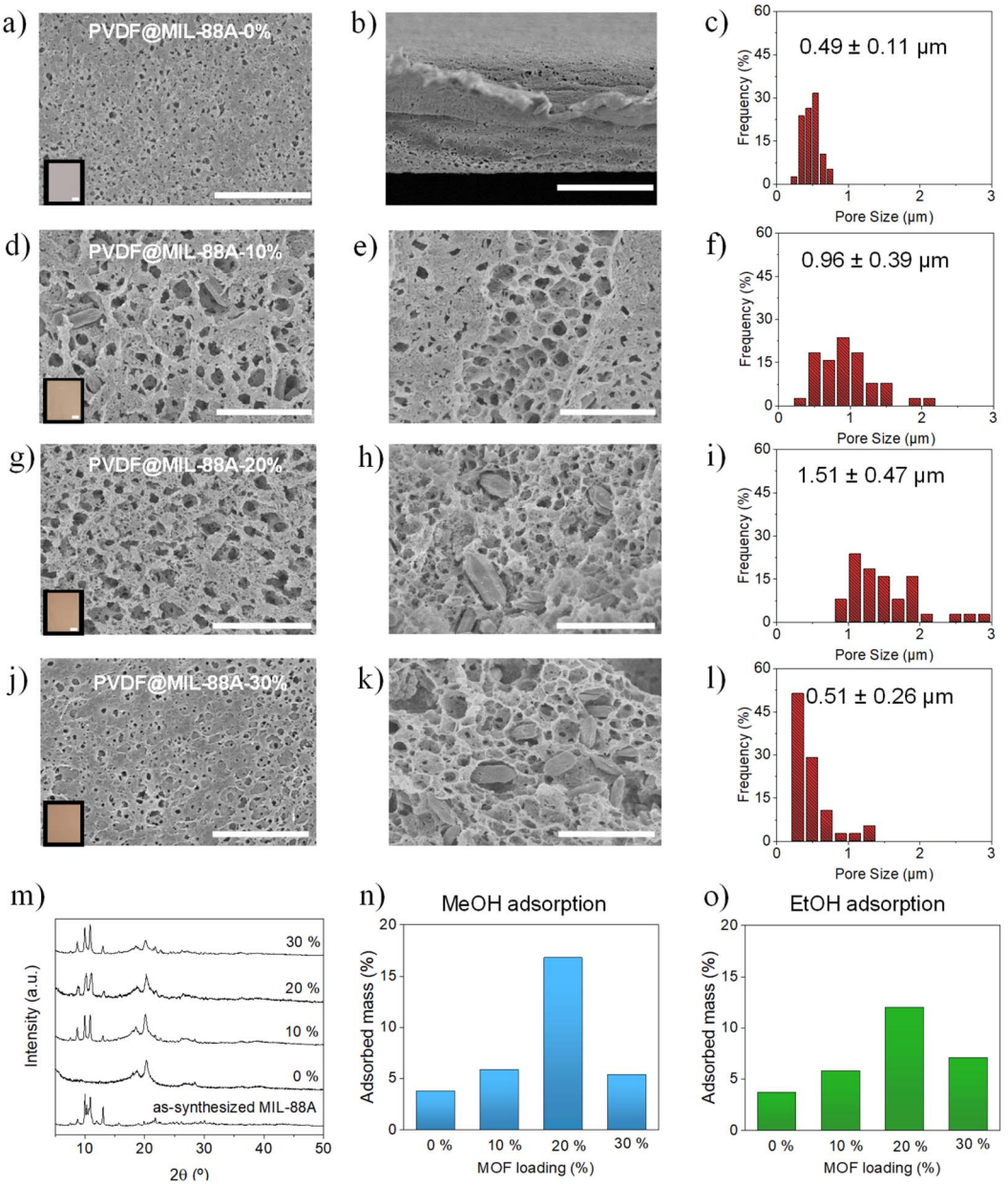

Fig. 8 SEM images (scale bar: 10 μm) for pore size and morphology characterization of PVDF@MIL-88A(Fe) membranes and captured images (inset figure, scale bar: 1 cm) with different MOF loadings: (a, d, g, j) surface, (b, e, h, k) cross section and (c, f, i, l) pore-size distribution and average pore size of 0, 10, 20 and 30 wt% MOF-loaded membranes, respectively. (m) PXRD of MIL-88A(Fe) and prepared membranes. Adsorption of alcohols from water in PVDF@MIL-88A(Fe) membranes: (n) methanol and (o) ethanol.

was employed to confirm the MOF content in the membrane. Furthermore, contact angle measurements showed that the hydrophilic nature of the PVDF membranes is decreased after the incorporation of MIL-88A(Fe), which agrees with the greater preference towards the more hydrophobic alcohols observed in the competitive adsorption studies.

The methanol and ethanol adsorption performances of the PVDF@MIL-88A(Fe) membranes were analyzed by ^{1}H-NMR spectroscopy (Fig. S15–S24†). The experiments were performed using a very dilute aqueous solution (0.1 wt%) of both alcohols in order to study the removal capacity of low-concentration alcohols from water (Fig. 8n and o). In both cases, the higher adsorption was observed for the 20 wt% MOF-loaded membrane: 17% and 12% for methanol and ethanol, respectively. This excellent performance of the 20 wt% membrane could be attributed to the intrinsic adsorptive properties of MIL-88A(Fe) as well as the higher porosity of the polymeric PVDF matrix that ensures better accessibility for the adsorbate molecules. The sharp decrease of the porosity in the polymeric matrix can be the reason for the poor adsorptive performance of the membrane with a 30 wt% of MOF. On the other hand, the results obtained for the 20 wt%-loaded

PVDF@MIL-88A(Fe) membrane clearly exceed the expected adsorption capacity based on the MIL-88A(Fe) adsorption results on single alcohols and the adsorption of the pure PVDF membrane. This fact is indicative of the synergetic contribution from both the MIL-88A(Fe) microcrystals and PVDF matrix which in combination result in the higher porosity as well as the more hydrophobic nature of the membrane. Furthermore, the 20 wt%-loaded PVDF@MIL-88A(Fe) membranes were regenerated *via* treating under vacuum for 90 min each in order to evaluate their recyclability. To our delight, the 20 wt%-loaded membrane showed significant recyclability up to 4 cycles toward both MeOH and EtOH (Fig. S25†).

Conclusion

In this work we have analyzed how the flexible nature of the crystal structure of MIL-88A(Fe) impacts on its adsorptive performance for the recovery of alcohols from water. Taking advantage of the paramagnetic nature of MIL-88A(Fe), a convenient magnetic sustentation technique was employed for the quantification of the captured alcohol mass. The results show the tendency for the linear alcohols, in which greater adsorption values are shown for the smaller alcohol molecule (methanol) due to a more efficient occupation of the void volume. However, this trend is not observed for the branched alcohols, where more modest adsorption values are shown. In this case, the adsorption is related to the cross-section (contrary to linear alcohols, where molecular volume is the limiting factor), suggesting an adsorption phenomenon dominated by diffusional aspects. In fact, the computational analysis of the pore system in the open form of MIL-88A(Fe) revealed that although the windows connecting these cavities are narrow, the cavities are big enough to accommodate these branched alcohols. In addition, considering the cross-section of the adsorbate molecules, even the linear alcohols with the smaller cross-section would not be able to go through them if the crystal structure would be rigid. However, the flexible structure of MIL-88A(Fe) is able to overcome this apparent diffusional problem in the case of the linear alcohols but hardly for branched alcohols. This diffusional challenge also plays a crucial role on the adsorption selectivity, as the hydrophobic nature of MIL-88A(Fe) favors a stronger interaction with the *tert*-butyl alcohol molecules on the outer surface of the adsorbent. These molecules start diffusing through the pore system of MIL-88A(Fe) but the mentioned diffusional problem leads to a clogging effect that hinders the entering of methanol molecules, a counterintuitive result based on the data coming from the single alcohol adsorption experiments but confirmed through consecutive single alcohol adsorption experiments.

Overall, MIL-88A(Fe) was strategically utilized in this work for selective alcohol recovery from water owing to its guest-induced breathing mediated structural adaptability. Furthermore, the sorption properties of MIL-88A(Fe) found to vary depending upon the nature of the sorbent solution, *i.e.* single-component or mixture alcohol solution. Such important findings are further supported by the theoretical and experimental studies revealing that the framework flexibility and diffusion play a key role in alcohol adsorption for MIL-88A(Fe). Furthermore, processability aspect of the power MOF materials has been addressed by preparing PVDF@MIL-88A(Fe) membranes. The synergistic effect of the polymeric matrix and the incorporated MIL-88A(Fe) microcrystals resulted in an increment in the adsorption capacity of the PVDF@MIL-88A(Fe) composite material compared to the performance of each component, independently. We believe that the results acquired in this work can open new avenues toward rational designing and potential utilization of flexible MOF-based systems offering enhanced selectivity and sorption performance toward the challenging liquid–liquid separation. Such adaptive systems can be extremely crucial and even a potential game changer towards designing of multipurpose standalone sorbent materials for size selective separation applications.

Conflicts of interest

There are no conflicts to declare.

Acknowledgements

This work was supported by the Spanish State Research Agency (AEI) and the European Regional Development Fund (ERFD) through the project PID2020–15935RB-C42. The European Union's Horizon 2020 research and Innovation programmes is also acknowledged for the funding of the LC-SC3-RES-25-2020 4AirCRAFT (ref. 101022633) project. In addition, 4AirCRAFT project was also supported by Japan Science and Technology Agency (JST) and Mission Innovation Challenge was supported by the Sao Paulo Research Foundation (FAPESP).

Notes and references

1 M. Balat and H. Balat, *Energy Convers. Manage.*, 2008, **49**(10), 2727–2741.
2 M. Balat, H. Balat and C. Öz, *Prog. Energy Combust. Sci.*, 2008, **34**(5), 551–573.
3 M. Al-Sabawi, J. Chen and S. Ng, *Energy Fuels*, 2012, **26**(9), 5355–5372.
4 A. Shigematsu, T. Yamada and H. Kitagawa, *J. Am. Chem. Soc.*, 2012, **134**(32), 13145–13147.
5 L.-H. Xu, S.-H. Li, H. Mao, Y. Li, A.-S. Zhang, S. Wang, W.-M. Liu, J. Lv, T. Wang, W.-W. Cai, L. Sang, W.-W. Xie, C. Pei, Z.-Z. Li, Y.-N. Feng and Z.-P. Zhao, *Science*, 2022, **378**(6617), 308–313.
6 J. Hill, E. Nelson, D. Tilman, S. Polasky and D. Tiffany, Environmental, economic, and energetic costs and benefits of biodiesel and ethanol biofuels, *PNAS*, 2006, **103**(30), 11206–11210, DOI: 10.1073/pnas.0604600103.
7 H.-J. Huang, S. Ramaswamy, U. W. Tschirner and B. V. Ramarao, *Sep. Purif. Technol.*, 2008, **62**(1), 1–21.
8 A. Nalaparaju, X. S. Zhao and J. W. Jiang, *Energy Environ. Sci.*, 2011, **4**(6), 2107.
9 S. C. Lee, H. W. Oh, H. C. Woo and Y. H. Kim, *Biomass Convers. Biorefin.*, 2021, **56**, 289.

10 Y. Q. Ma, H. Z. Ma, L. Zheng, J. Yang, Y. F. Liu and Q. H. Wang, *Appl. Mech. Mater.*, 2013, **448–453**, 540–544.
11 S. Mukherjee, D. Sensharma, O. T. Qazvini, S. Dutta, L. K. Macreadie, S. K. Ghosh and R. Babarao, *Coord. Chem. Rev.*, 2021, **437**, 213852.
12 B. van de Voorde, B. Bueken, J. Denayer and D. de. Vos, *Chem. Soc. Rev.*, 2014, **43**(16), 5766–5788.
13 T. C. Bowen and L. M. Vane, *Langmuir*, 2006, **22**(8), 3721–3727.
14 Z. Jia and G. Wu, *Microporous Mesoporous Mater*, 2016, **235**(1–2), 151–159.
15 F. Ahmadijokani, H. Molavi, S. Tajahmadi, M. Rezakazemi, M. Amini, M. Kamkar, O. J. Rojas and M. Arjmand, *Coord. Chem. Rev.*, 2022, **464**, 214562.
16 R. Freund, U. Lächelt, T. Gruber, B. Rühle and S. Wuttke, *ACS nano*, 2018, **12**(3), 2094–2105, DOI: **10.1021/acsnano.8b00932**.
17 H.-C. J. Zhou and S. Kitagawa, *Chem. Soc. Rev.*, 2014, **43**(16), 5415–5418, DOI: **10.1039/c4cs90059f**.
18 P. Z. Moghadam, A. Li, S. B. Wiggin, A. Tao, A. G. P. Maloney, P. A. Wood, S. C. Ward and D. Fairen-Jimenez, *Chem. Mater.*, 2017, **29**(7), 2618–2625.
19 M. Safaei, M. M. Foroughi, N. Ebrahimpoor, S. Jahani, A. Omidi and M. Khatami, *TrAC, Trends Anal. Chem.*, 2019, **118**, 401–425.
20 U. Mueller, M. Schubert, F. Teich, H. Puetter, K. Schierle-Arndt and J. Pastré, *J. Mater. Chem.*, 2006, **16**(7), 626–636.
21 A. J. Blake, N. R. Champness, P. Hubberstey, W. Li, M. A. Withersby and M. Schröder, *Coord. Chem. Rev.*, 1999, **183**(117), 117–138.
22 H.-L. Zhou, R.-B. Lin, C.-T. He, Y.-B. Zhang, N. Feng, Q. Wang, F. Deng, J.-P. Zhang and X.-M. Chen, *Nat. Commun.*, 2013, **4**, 2534.
23 A. U. Czaja, N. Trukhan and U. Müller, *Chem. Soc. Rev.*, 2009, **38**(5), 1284–1293.
24 R. Freund, O. Zaremba, G. Arnauts, R. Ameloot, G. Skorupskii, M. Dincă, A. Bavykina, J. Gascon, A. Ejsmont, J. Goscianska, M. Kalmutzki, U. Lächelt, E. Ploetz, C. S. Diercks and S. Wuttke, *Angew. Chem. Int. Ed.*, 2021, **60**(45), 23975–24001.
25 R. Freund, S. Canossa, S. M. Cohen, W. Yan, H. Deng, V. Guillerm, M. Eddaoudi, D. G. Madden, D. Fairen-Jimenez, H. Lyu, L. K. Macreadie, Z. Ji, Y. Zhang, B. Wang, F. Haase, C. Wöll, O. Zaremba, J. Andreo, S. Wuttke and C. S. Diercks, *Angew. Chem. Int. Ed.*, 2021, **60**(45), 23946–23974.
26 Z. Ji, H. Wang, S. Canossa, S. Wuttke and O. M. Yaghi, *Adv. Funct. Mater.*, 2020, **30**(41), 2000238.
27 R. Kitaura, K. Fujimoto, S.-i. Noro, M. Kondo and S. Kitagawa, *Angew. Chem. Int. Ed.*, 2002, **41**(1), 133–135.
28 C. Serre, F. Millange, C. Thouvenot, M. Noguès, G. Marsolier, D. Louër and G. Férey, *J. Am. Chem. Soc.*, 2002, **124**(45), 13519–13526.
29 G. Férey and C. Serre, *Chem. Soc. Rev.*, 2009, **38**(5), 1380–1399.
30 T. Devic, P. Horcajada, C. Serre, F. Salles, G. Maurin, B. Moulin, D. Heurtaux, G. Clet, A. Vimont, J.-M. Grenèche, B. Le Ouay, F. Moreau, E. Magnier, Y. Filinchuk, J. Marrot, J.-C. Lavalley, M. Daturi and G. Férey, *J. Am. Chem. Soc.*, 2010, **132**(3), 1127–1136.
31 P. G. Yot, Q. Ma, J. Haines, Q. Yang, A. Ghoufi, T. Devic, C. Serre, V. Dmitriev, G. Férey, C. Zhong and G. Maurin, *Chem. Sci.*, 2012, **3**(4), 1100, DOI: **10.1039/c2sc00745b**.
32 E. Virmani, O. Beyer, U. Lüning, U. Ruschewitz and S. Wuttke, *Mater. Chem. Front.*, 2017, **1**(10), 1965–1974.
33 J. H. Lee, S. Jeoung, Y. G. Chung and H. R. Moon, *Coord. Chem. Rev.*, 2019, **389**, 161–188.
34 S. Seth and S. Jhulki, *Mater. Horiz.*, 2021, **8**(3), 700–727.
35 Z. Chang, D.-H. Yang, J. Xu, T.-L. Hu and X.-H. Bu, *Adv. Mater.*, 2015, **27**(36), 5432–5441.
36 X.-N. Cheng, W.-X. Zhang, Y.-Y. Lin, Y.-Z. Zheng and X.-M. Chen, *Adv. Mater.*, 2007, **19**(11), 1494–1498.
37 F. Salles, G. Maurin, C. Serre, P. L. Llewellyn, C. Knöfel, H. J. Choi, Y. Filinchuk, L. Oliviero, A. Vimont, J. R. Long and G. Férey, *J. Am. Chem. Soc.*, 2010, **132**(39), 13782–13788.
38 J.-P. Zhang and X.-M. Chen, *J. Am. Chem. Soc.*, 2008, **130**(18), 6010–6017.
39 Z. Wang and S. M. Cohen, *J. Am. Chem. Soc.*, 2009, **131**(46), 16675–16677.
40 L. R. Parent, C. H. Pham, J. P. Patterson, M. S. Denny, S. M. Cohen, N. C. Gianneschi and F. Paesani, *J. Am. Chem. Soc.*, 2017, **139**(40), 13973–13976.
41 T. Chalati, P. Horcajada, R. Gref, P. Couvreur and C. Serre, *J. Mater. Chem.*, 2011, **21**(7), 2220–2227.
42 P. Hirschle, C. Hirschle, K. Böll, M. Döblinger, M. Höhn, J. M. Tuffnell, C. W. Ashling, D. A. Keen, T. D. Bennett, J. O. Rädler, E. Wagner, M. Peller, U. Lächelt and S. Wuttke, *Chem. Mater.*, 2020, **32**(6), 2253–2263.
43 P. Horcajada, F. Salles, S. Wuttke, T. Devic, D. Heurtaux, G. Maurin, A. Vimont, M. Daturi, O. David, E. Magnier, N. Stock, Y. Filinchuk, D. Popov, C. Riekel, G. Férey and C. Serre, *J. Am. Chem. Soc.*, 2011, **133**(44), 17839–17847.
44 N. A. Ramsahye, T. K. Trung, L. Scott, F. Nouar, T. Devic, P. Horcajada, E. Magnier, O. David, C. Serre and P. Trens, *Chem. Mater.*, 2013, **25**(3), 479–488.
45 A. C. McKinlay, J. F. Eubank, S. Wuttke, B. Xiao, P. S. Wheatley, P. Bazin, J.-C. Lavalley, M. Daturi, A. Vimont, G. de Weireld, P. Horcajada, C. Serre and R. E. Morris, *Chem. Mater.*, 2013, **25**(9), 1592–1599.
46 H. Wu, M.-D. Ma, W.-Z. Gai, H. Yang, J.-G. Zhou, Z. Cheng, P. Xu and Z.-Y. Deng, *Environmental science and pollution research international*, 2018, **25**(27), 27196–27202.
47 Z. Zhang, Y. Chen, Z. Wang, C. Hu, D. Ma, W. Chen and T. Ao, *Applied Surface Science*, 2021, **542**, 148662.
48 W.-T. Xu, L. Ma, F. Ke, F.-M. Peng, G.-S. Xu, Y.-H. Shen, J.-F. Zhu, L.-G. Qiu and Y.-P. Yuan, *Dalton transactions*, 2014, **43**(9), 3792–3798.
49 J. C. Barbosa, R. Gonçalves, A. Valverde, P. M. Martins, V. I. Petrenko, M. Márton, A. Fidalgo-Marijuan, R. Fernández de Luis, C. M. Costa and S. Lanceros-Méndez, *Chem. Eng. J.*, 2022, **443**(12), 136329.
50 C. Ribeiro, C. M. Costa, D. M. Correia, J. Nunes-Pereira, J. Oliveira, P. Martins, R. Gonçalves, V. F. Cardoso and S. Lanceros-Méndez, *Nat. Protoc.*, 2018, **13**(4), 681–704.

51 J. Troyano, A. Carné-Sánchez, J. Pérez-Carvajal, L. León-Reina, I. Imaz, A. Cabeza and D. Maspoch, *Angew. Chem. Int. Ed.*, 2018, **130**(47), 15646–15650.
52 R. Pérez-Aguirre, B. Artetxe, G. Beobide, O. Castillo, I. de Pedro, A. Luque, S. Pérez-Yáñez and S. Wuttke, *Cell Rep. Phys. Sci*, 2021, **2**(5), 100421.
53 N. Barroso, J. Andreo, G. Beobide, O. Castillo, A. Luque, S. Perez-Yáñez and S. Wuttke, *Commun. Chem.*, 2023, **6**(4), 1–9.
54 P. Nugent, Y. Belmabkhout, S. D. Burd, A. J. Cairns, R. Luebke, K. Forrest, T. Pham, S. Ma, B. Space, L. Wojtas, M. Eddaoudi and M. J. Zaworotko, *Nature*, 2013, **495**(7439), 80–84.
55 M. Hmoudah, A. El-Qanni, R. Tesser, R. Esposito, A. Petrone, O.-S. Jung, T. Salmi, V. Russo and M. Di Serio, *Materials Science and Engineering: B*, 2023, **288**(5), 116179.
56 J. Ren, N. M. Musyoka, H. W. Langmi, A. Swartbooi, B. C. North and M. Mathe, *Int. J. Hydrogen Energy*, 2015, **40**(13), 4617–4622.
57 S. Yu, H. Pang, S. Huang, H. Tang, S. Wang, M. Qiu, Z. Chen, H. Yang, G. Song, D. Fu, B. Hu and X. Wang, *Sci. Total Environ.*, 2021, **800**, 149662.
58 Z. Jia and G. Wu, *Microporous Mesoporous Mater*, 2016, **235**(1–2), 151–159.
59 S. J. Datta, A. Mayoral, N. Bettahalli, P. M. Bhatt, M. Karunakaran, I. D. Carja, D. Fan, P. Mileo, R. Semino, G. Maurin, O. Terasaki and M. Eddaoudi, *Science*, 2022, **376**, 1–8, DOI: **10.1126/science.abe0192**.
60 S. Zhou, O. Shekhah, J. Jia, J. Czaban-Jóźwiak, P. M. Bhatt, A. Ramírez, J. Gascon and M. Eddaoudi, *Nat. Energy*, 2021, **6**(9), 882–891.
61 X. Wang, L. Zhai, Y. Wang, R. Li, X. Gu, Y. Di Yuan, Y. Qian, Z. Hu and D. Zhao, *ACS Appl. Mater. Interfaces*, 2017, **9**(43), 37848–37855.
62 J. E. Efome, D. Rana, T. Matsuura and C. Q. Lan, *ACS Appl. Mater. Interfaces*, 2018, **10**(22), 18619–18629.
63 T. A. Makhetha and R. M. Moutloali, *J. Membr. Sci.*, 2018, **554**, 195–210.
64 Z. Li, P. Yang, Z. Gao, M. Song, Q. Fang, M. Xue and S. Qiu, *Chem. Commun.*, 2019, **55**(24), 3505–3508.
65 Y. Deng, Y. Wu, G. Chen, X. Zheng, M. Dai and C. Peng, *Chem. Eng. J.*, 2021, **405**, 127004.
66 J. Gu, H. Fan, C. Li, J. Caro and H. Meng, *Angew. Chem. Int. Ed.*, 2019, **58**(16), 5297–5301.
67 T. A. Otitoju, A. L. Ahmad and B. S. Ooi, *J. Water Process Eng.*, 2016, **14**(5849), 41–59, DOI: **10.1016/j.jwpe.2016.10.011**.
68 A. Valverde, R. Gonçalves, M. M. Silva, S. Wuttke, A. Fidalgo-Marijuan, C. M. Costa, J. L. Vilas-Vilela, J. M. Laza, M. I. Arriortua, S. Lanceros-Méndez and R. Fernández de Luis, *ACS Appl. Energy Mater.*, 2020, **3**(12), 11907–11919.
69 P. Martins, A. C. Lopes and S. Lanceros-Mendez, *Prog. Polym. Sci.*, 2014, **39**(4), 683–706.
70 P. Thakur, A. Kool, B. Bagchi, S. Das and P. Nandy, *Phys. Chem. Chem. Phys.*, 2015, **17**(2), 1368–1378.